Advances in Aircraft and Spacecraft Science, *Vol. 10, No. 6 (2023) 555-572*
https://doi.org/10.12989/aas.2023.10.6.555

Experimental studies of damage to aircraft skin under the influence of raindrops

Minggong Sha[1,2,3a], Ying Sun[4b], Li Yulong[1,2,3c], Vladimir I. Goncharenko[4d], Vladimir S. Oleshko[4e], Anatoly V. Ryapukhin[*4] and Victor M. Yurov[5f]

[1]*School of Civil Aviation, Northwestern Polytechnical University, Xi'an 710072, Shaanxi, China*
[2]*Shaanxi Impact Dynamics and Engineering Application Laboratory, Xi'an 710072, Shaanxi, China*
[3]*NPU Yangtze River Delta Research Institute, 215400 Suzhou, China*
[4]*Moscow Aviation Institute, Volokolamskoe Highway 4, 125993 Moscow, Russia*
[5]*Karaganda Technical University, Nazarbaev Street 56, 100056 Karaganda, Kazakhstan*

(Received December 19, 2023, Revised January 31, 2024, Accepted February 11, 2024)

Abstract. Airplanes in flight collide with raindrops, and the leading edges of the airframe can be damaged when colliding with raindrops. A single waterjet testing platform was created to study rain erosion damage. Carbon fiber samples with three types of skins were studied and the mechanical properties were measured using a nanoindentation instrument. The research results show that the impact force on the sample increases with the continuous increase in the impact speed of raindrops, which leads to an increase in the damage area. Sheathing with low surface roughness is more damaged than other sheathings due to its rougher surface, and the result proves that surface roughness has a more significant effect on rain erosion damage to sheathings compared to their hardness.

Keywords: coating; composite material; impact dynamics; rain erosion damage; single jet

1. Introduction

When an object (supersonic aircraft, missile, propeller blade) passes through the rain area at high speed, the phenomenon that the surface is damaged by the impact of raindrops is called rain erosion. The damage caused by rain erosion can be divided into structural strength damage and functional damage (Jenkins 1955, Kennedy and Field 2000). Usually, rain erosion damage is not obvious at the initial stage. But it will cause the degradation of material strength, the reduction of physical or mechanical properties, and even local coating is spalled, which will affect the functional characteristics of the structure, and will significantly reduce the strength of the structure in severe cases.

*Corresponding author, Professor, E-mail: ryapukhin.a.v@mail.ru
[a]Professor, E-mail: miggongsha@gmail.com
[b]Professor, E-mail: yingsunhangzhou@gmail.com
[c]Professor, E-mail: yulongli731@gmail.com
[d]Professor, E-mail: goncharenko_vi@mail.ru
[e]Professor, E-mail: okeshkovlad@mail.ru
[f]Professor, E-mail: vicyurov@mail.ru

http://www.techno-press.org/?journal=aas&subpage=7 ISSN: 2287-528X (Print), 2287-5271 (Online)

With the gradual increase of the flight speed of the aircraft, the coatings of the aircraft's external fairing, windshield, and the leading edge of the tail will be severely impacted by raindrops during the long-term service process, resulting in bubbles, cracks, softening, and peeling of the coating, discoloration, powdering and other phenomena (Field *et al.* 1989, Field, 1986, Itoh and Okabe 1993, Richman 2002, Li 2008). The rain erosion resistance of aircraft skin coating is one of the indicators to consider its main function (Lan *et al.* 2014), and the failure of the coating is likely to lead to aircraft quality and safety accidents, such as the failure of the aircraft fuel tank coating, which will lead to oil leakage in the fuel tank, The peeling off of the first functional coating will cause the engine to be damaged by the impact of foreign objects. At the same time, the eroded surface will seriously affect the laminar flow effect of the aircraft wing, resulting in laminar flow turning to turbulent flow, which will have a serious negative impact on the aerodynamic performance of the aircraft, thereby increasing fuel consumption (Young and Humphreys 2001). Coto (Coto *et al.* 2021) *et al.* used carbon fiber reinforced polymer as the matrix and used Physical Vapor Deposition (Physical Vapor Deposition, PVD) single-layer/multi-layer titanium coating to conduct impact resistance tests under rain erosion conditions. The test results show that the coating thickness and surface adhesion will affect the protective performance of the coating under different rain erosion conditions, and high-speed impact will cause greater substrate deformation, even on thicker coating surfaces, due to it adheres poorly and peels off faster than thinner coatings. Gujba (Gujba *et al.* 2016) studied the droplet erosion behavior and material damage mechanism of Ti-6Al-4V materials. It is considered that the higher impact velocity, the faster erosion initiation time and the greater maximum erosion rate. Using scanning electron microscopy to observe the two stages of erosion damage formation: the early main morphology is microcracks, coarse cracks and irregular pits, while in the later stage of droplet erosion, the damage morphology of the material is mainly peeling, what caused by hydraulic infiltration. Jakob (Bech *et al.* 2022) studied the influence of four droplet diameters on the rain erosion results of commercial turbine blade polyurethane-based topcoats in RET-Rain Erosion Tests and established the relation between droplet size and topcoat life. The empirical model among them verified that the raindrop diameter is one of the main parameters affecting the degree of leaf damage (Mednikov *et al.* 2021).

In addition, helicopter blades, advanced aero-engine fans and other composite multi-phase material blades, rain erosion becomes the One of the main natural causes of cracking due to a certain probability of manufacturing defects in production, such as roughness, porosity, etc. The tensile shear fatigue failure caused by the high-speed impact of raindrops on the surface paint defects leads to leading edge erosion (Leading edge erosion, LEE), resulting in fatigue erosion damage to the coating, and the matrix at the leading edge. However, due to the lack of theoretical and experimental studies on rain erosion damage failure, there is no well-defined method to design rain erosion resistant coatings (Ying and Xu 2011, Schramm *et al.* 2017, Valaker *et al.* 2015, Schmitt 1974, King 1976, Slot *et al.* 2015, Zhang *et al.* 2015, Keegan *et al.* 2013). Adler (1999) pointed out that one of the difficulties in the study of rain erosion is that it is difficult to establish a reasonable theory in the short term for the problem of material peeling. It is also difficult to construct a unified relation between microstructural mechanics, droplet impact failure, and material detachment. To sum up, in the manufacturing process of high-speed aircraft and industrial impellers, higher requirements are put forward for the rain erosion resistance of the coating (Field *et al.* 1989, Slot *et al.* 2015, Mishnaevsky 2019). Therefore, it is of great engineering significance to study the failure test of coatings of rain erosion damage.

Surface and subsurface defects in aircraft skin can be detected visually, acoustically or by X-ray non-destructive testing methods.

Thus, in this paper, in contrast to the previous works of the authors cited here, we carried out impact tests of the aircraft skin, analyzed the morphology of damage resulting from the impact of a high-speed jet and the mechanism of damage. The purpose of the work is to obtain new knowledge on the theoretical and technical support for the design of aircraft linings that are resistant to rain erosion.

2. Materials and methods

2.1 High-speed ımpact process between raindrops and aircraft skin coating

The high-speed impact process of raindrops on aircraft skin coating is actually the propagation process of dynamic shock waves generated by raindrops directly hitting the solid surface. The shock process consists of two stages, namely the initial compression stage and the side injection stage. When the droplet hits the surface of the material at a normal angle, the droplet deforms after impact, generating a Rayleigh wave propagating along the solid surface, containing about 2/3 of the collision energy, forming tensile stress and Shear stress (Gohardani 2011). The damaged area inside the solid will form a longitudinal wave and a shear wave, which propagate into the liquid and the solid, respectively. The longitudinal wave propagates in the form of compression-tension, and when the wave front expands rapidly, radial tensile stress will be generated. In the shear wave, the particle motion is perpendicular to the propagation direction which will cause shear stress and hoop tensile stress inside the solid (Zahavi and Nadiv 1981). At this time, the diffusion velocity of the liquid-solid contact boundary is greater than the propagation velocity of the stress wave inside the liquid, and the central liquid is compressed to form a transient high pressure, which is called "water hammer pressure". The duration of water hammer pressure is very short, which is related to parameters such as droplet diameter, impact velocity, and compressible wave velocity, and its magnitude has nothing to do with the droplet diameter (Cook 1928, Heymann 1968). The stress generated during the liquid-solid impact causes the initiation and expansion of material damage, and the reflection of the stress wave on the free surface and the interaction inside the solid will lead to the superposition and enhancement of the wave, thus causing damage inside the solid.

Among them, the water hammer pressure p can be expressed by the equation (predict the pressure generated in the initial stage of contact) (Dear and Field 1988)

$$p = \frac{\rho_l C_l \rho_s C_s v}{\rho_l C_l + \rho_s C_s}, \tag{1}$$

where v is the impact velocity of the droplet, ρ_l and ρ_s are the densities of the liquid and solid matrix, respectively, and c_l and c_s are the propagation speeds of sound in the liquid and solid, respectively.

When the shock wave velocity inside the droplet is about to exceed the expansion velocity of the liquid-solid contact boundary, the shock wave breaks away from the boundary, and the internal high pressure is released in the form of a high-speed lateral jet. The scouring and shearing effect of the lateral jet on the surface of the material will lead to the appearance of cracks, and even cause the surface of the material to peel off. The liquid then forms a steady incompressible flow on the solid surface, at which point the pressure at the contact center point drops to the Bernoulli static pressure.

Post-impact shock waves also propagate through the material hierarchically through multiple

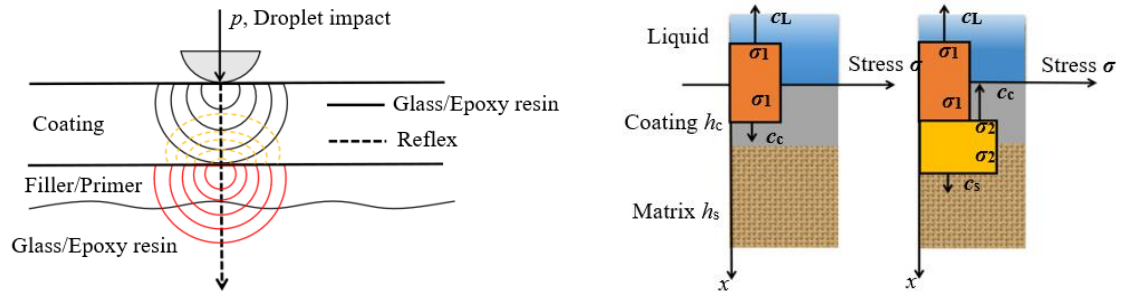

(a) Standard blade structure with a filler intermediate layer (b) Normal shockwave propagation depending on acoustic impedances in two consecutive time instants

Fig. 1 The process of shock wave passage: (a) Standard blade structure with a filler intermediate layer

layers, and the resulting damage depends on factors such as material elastic and viscoelastic responses, surface preparation, coating application and interlayer interactions. The reflection and transmission propagation process of the stress wave on the surface of the coating and the substrate is shown in the Fig. 1(a). When in contact with the coating, two different wave fronts enter the liquid and the coating respectively, as shown in Fig. 1(b), the normal incident wave in the coating propagates toward the coating-substrate interface, and part of the stress wave part is reflected back to the coating, while another part is transmitted into the substrate. Based on this reflection and transmission, the stress wave will propagate in the coating with different amplitudes, and its intensity depends on the relative magnitude of the acoustic impedance of the coating and the substrate (Springer 1974). Assuming that the one-dimensional elastic assumption is adopted, the approximate relation of the amplitude of the stress wave is obtained as

$$\frac{\sigma_{R_{LC}}}{\sigma_{I_{LC}}}=\frac{Z_L-Z_C}{Z_L+Z_C};\frac{\sigma_{T_{LC}}}{\sigma_{I_{LC}}}=\frac{2Z_C}{Z_L+Z_C}, \tag{2}$$

$$\frac{\sigma_{R_{CS}}}{\sigma_{I_{CS}}}=\frac{Z_C-Z_S}{Z_C+Z_S};\frac{\sigma_{T_{CS}}}{\sigma_{I_{CS}}}=\frac{2Z_S}{Z_C+Z_S}. \tag{3}$$

Among them, $Z=\rho c$ is the impedance of the material, ρ is the density, and c is the stress wave velocity (the sound velocity of the medium). Z_L, Z_C and Z_S represent the impedance of the liquid (L), coating (C) and substrate (S), respectively. $\sigma_{ILC}, \sigma_{RLC}, \sigma_{TLC}$ are the amplitudes of the normally incident, reflected and transmitted stress waves at the liquid-coating interface, respectively, $\sigma_{ICS}, \sigma_{RCS}, \sigma_{TCS}$ are the amplitudes of the normally incident, reflected and transmitted stress waves at the coating-substrate interface, respectively.

3. Results and discussion

3.1 Rain erosion test process

3.1.1 Single jet simulated rain erosion test platform

The experimental devices for researching the failure behavior of aircraft skin coating rain erosion damage can be divided into two types according to the test speed requirements: (1) In

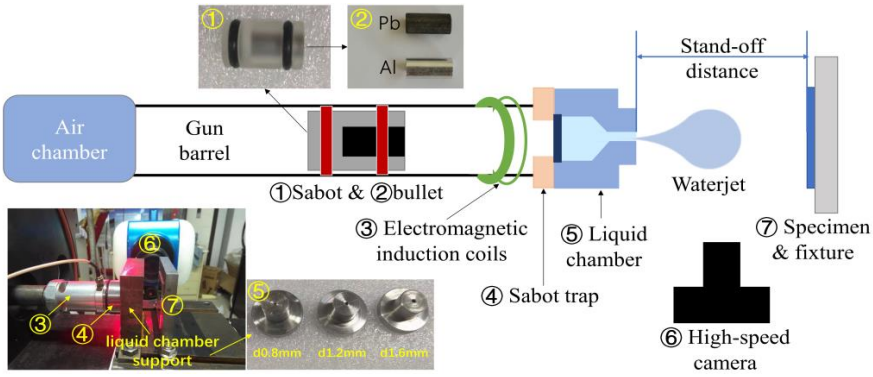

Fig. 2 Single impact waterjet apparatus

order to study the rain erosion resistance of materials under the impact of continuous raindrops whose speed is usually less than 250 m/s, the experimental usually take a rotating arm devices (Tobin *et al.* 2011). The device is low in cost and can simulate the damage of the sample in the real rain field, but the size and speed of the sample are limited by the strength of the rotating arm, (2) for the impact test of raindrops at supersonic speed and the speed is less than 1000 m/s, under laboratory conditions, a single-jet simulation rain erosion device is usually used (Adler 1999, Obara *et al.* 1995), which is mainly used to study the basic mechanics of liquid-solid impact. The device has the advantages of small site, simple operation and controllable conditions.

According to the existing research data, based on the single impact jet apparatus (Single Impact Jet Apparatus, SIJA) jet launch principle of Cavendish Laboratory, the internal metal sheet impacts the liquid in the front nozzle at high speed through compressed air, which can produce water jet with speed 90-700 m/s. Therefore, this paper uses the high-speed jet generated by the single-drop jet device to study the raindrop impact damage behavior of the aircraft skin coating, as shown in the Fig. 2, including the air chamber, gun barrel, bullet, gasket, nozzle, tap water, fixture, High-speed cameras, etc. The working principle of the device: using high-pressure gas launch 5 mm lead bullets at a certain speed and the collision gasket squeezes the tap water in the sealing cavity to generate a high-speed jet. The device can simulate the impact process of raindrops on materials under multiple impact angles for liquid droplets with different impact velocities and diameters.

In order to be able to observe the shape of the jet and calculate the velocity of the jet, a Phantom VEO 1310 high-speed camera was used for shooting in the test. The impact velocity of the jet can be obtained by using the change of the front-end pixel of the ball jet and the relation between the calibration proof pixel and the distance

$$v = \frac{\upsilon(X_1 - X_2)}{1000N}. \tag{4}$$

Among them, v is the jet velocity, υ is the shooting frame rate, X_1 and X_2 are the starting point and end point of the droplet motion respectively, and N is the change in the number of pixels within 1 m displacement obtained through calibration. In this experiment, N=3.4×10^3 Pt/m, and the shooting frame rate is υ=210000 Hz.

The Fig. 3 shows the variation of jet velocity and shape with distance from the nozzle (with the nozzle as the origin): the jet velocity and jet diameter gradually increase at the initial stage, and then the jet head gradually becomes a stable spherical shape due to the effect of air resistance It

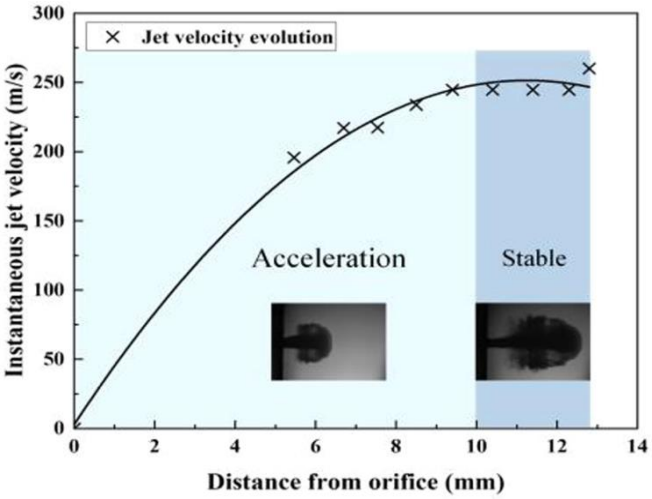

Fig. 3 Variation of the waterjet with stand-off distance

Table 1 Summary of experimental parameters

Sample material	Single impact velocity/(m·s^{-1})	Nozzle diameter/mm	Average jet diameter/mm
Polyurethane coating for aircraft skin	360 430 490 555 617	0.8	4.5

can be seen from the Fig. 3 that when the jet distance is 10 mm, the jet velocity and shape tend to be stable, and as the jet distance continues to increase, the jet shape gradually diverges. Therefore, based on the consideration of ensuring the repeatability and accuracy of the test, the sample was installed at a position 10 mm away from the nozzle. In order to ensure the repeatability of the test, at least three repeated tests were carried out at the same jet velocity. The parameters used in the experiment are presented in the Table 1.

3.1.2 Specifications and performance of aircraft skin polyurethane coating

Aircraft skin coatings mainly consist of chrome-free high solids epoxy primers and high solids polyurethane (PU) enamel. Among them, high solid content polyurethane enamel is divided into three categories: glossy enamel, semi-gloss enamel and matt enamel, and they are all belong to thermosetting polyurethane, which has excellent wear resistance and weather resistance. It is generally manufactured by spraying and widely used in aircraft manufacturing industry. The coating samples in this test are made of three different primers and enamel, all of which are based on 3 mm thick T300 carbon fiber braided material, the thickness of the primer is 200 μm, and the thickness of the enamel is 300 μm. Among them, material 1 is made of acrylic polyurethane primer and polyurethane matte enamel, material 2 is made of epoxy self-drying primer and acrylic polyaliphatic polyurethane enamel, material 3 is made of chrome-free high solid content epoxy primer and made of light high solids polyurethane enamel. The delamination of the original coating surface and its cross-section is shown in the Fig. 4, where A is the topcoat area, B is the

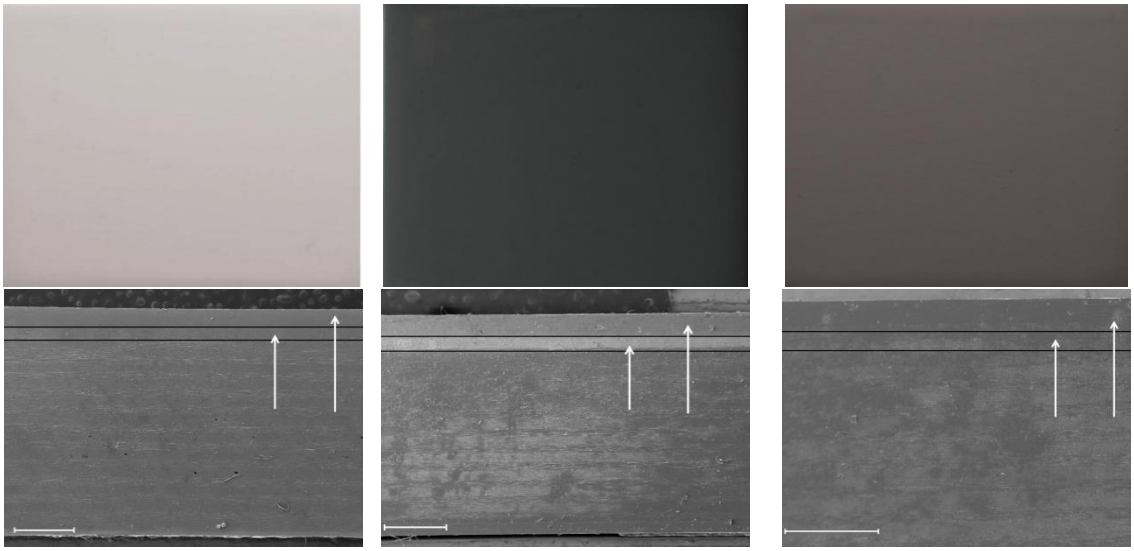

(a) Material 1 (b) Material 2 (c) Material 3

Fig. 4 Surface and cross-sections images of three kinds coatings

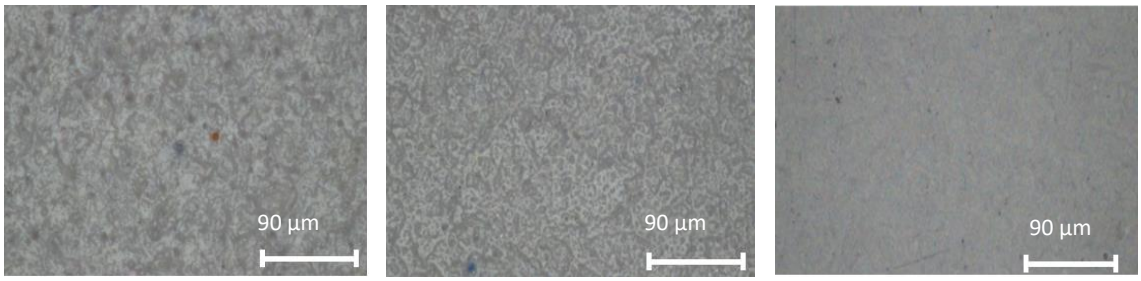

(a) Material 1 (b) Material 2 (c) Material 3

Fig. 5 Nano-indenter micrographs of the three kinds coatings

Table 2 Modulus and hardness comparison table of three kinds of coatings

Coating	Indentation modulus/GPa	Hardness/GPa
Material 1	5.806	0.240
Material 2	3.851	0.161
Material 3	2.414	0.111

primer area, and the rest is the substrate area.

In order to explore the influence of the mechanical properties of the coating on the rain erosion resistance, the coating performance was observed by using a Hysitron TI980 nano-indentation instrument. Among them, the surface roughness of the high-resolution sample is shown in the Fig. 5, and the roughness of the three coatings is material 1, material 2 and material 3 in sequence. The measured coating hardness and modulus data are shown in the Table 2. It can be seen that the modulus and hardness properties of each coating material are material 1, material 2, and material 3 from strong to weak. The greater hardness of a material with a higher roughness compared to a

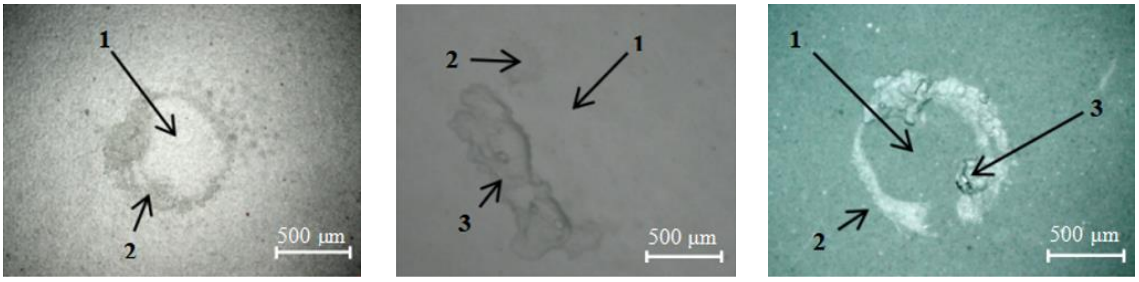

(a) Material 1 (b) Material 2 (c) Material 3

Fig. 6 Optical microscope micrographs of the three kinds coatings

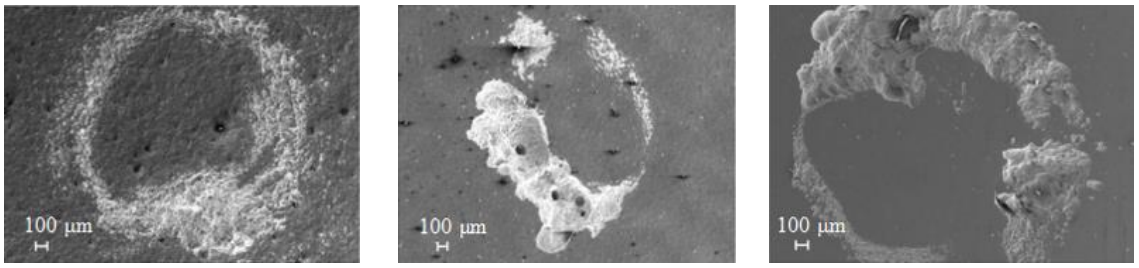

(a) Material 1 (b) Material 2 (c) Material 3

Fig. 7 SEM micrographs of the three kinds damage samples

material with a lower roughness is explained by the smaller depth of indentation of the nano-indenter relative to the nominal surface of the sample and, as a result, the smaller indentation area.

3.2 High-velocity jet ımpact test of aircraft coating

3.2.1 Typical damage modes and characterization of samples after impact

The Fig. 6 shows the microscopic images of typical microscopic damage morphology of three coating samples at the impact velocity of 490 m/s and impact angle of 0°. It can be seen that for the three different coating materials, the typical damage morphology is composed of a ring with a damaged area surrounding the central undamaged area (1), including surface scratches (2), irregular pits (3) and other progressive damage. The formation of this morphology is due to that the water hammer pressure does not cause damage to the central circular area because the superimposed hydrostatic pressure increases the yield strength of the coating surface, but as the droplet begins to compress and release, high pressure that 2-3 times the water hammer pressure will be generated at the liquid-solid contact boundary, resulting in surface depressions.

The Fig. 7 shows the microscopic topography images obtained by observing the typical damaged areas of the three coatings using SEM (Scanning Electron Microscope) scanning electron microscope. It can be seen that the typical microscopic morphology of the damaged area is ring-like damage.

3.2.2 Impact test results at different jet velocities

The Fig. 8 shows the electron microscopic morphology obtained by impacting the material 3 coating at the jet velocity of 360, 430, 490, 555 and 617 m/s at an impact angle of 15°. As the

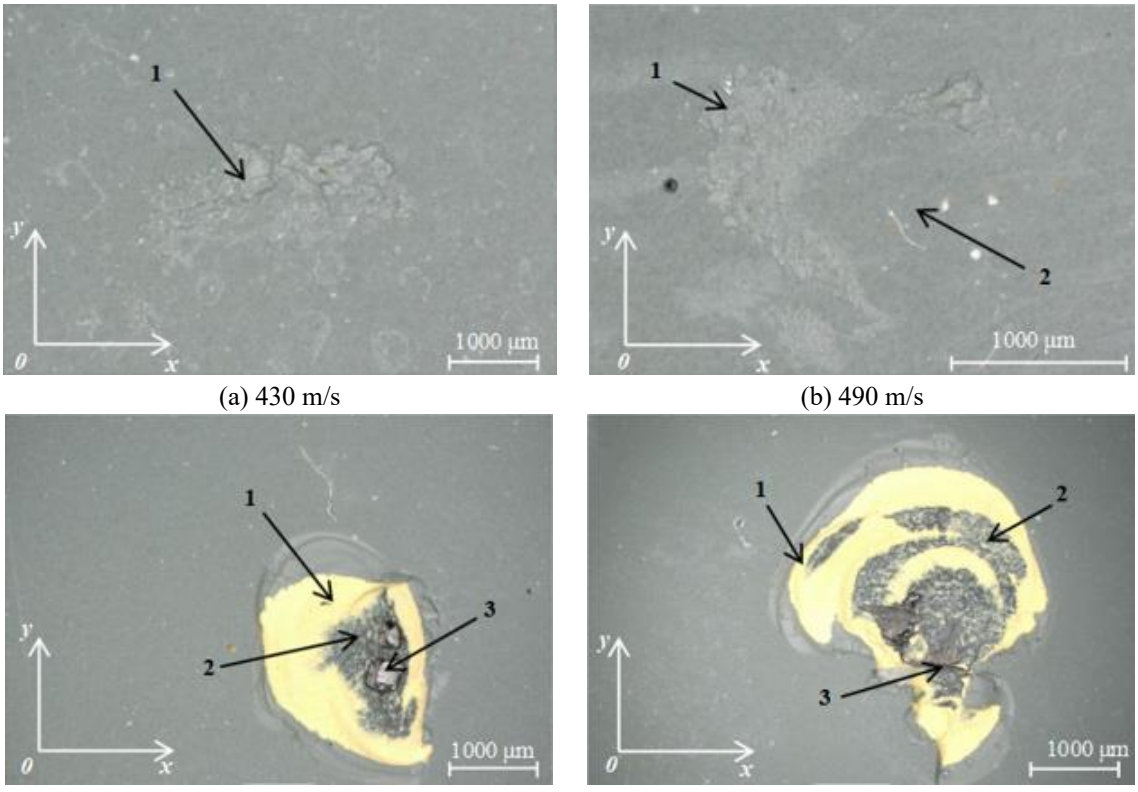

Fig. 8 Electron microscope micrographs after impacting the coating material 3 at the jet velocities of 360, 430, 490, 555 and 617 m/s atan impact angle of 0°

figure shows, at the impact speed of 360 m/s, the coating has no damage, so it is not displayed, from 430 m/s, slight scratches (1) appear on the coating surface, with a damage area of 0.76 mm^2, at the impact speed of 490 m/s, the damage situation is slightly intensified, the surface scratch area (1) increased to 1.18 mm^2, and the whole presents a semi-circle surrounding the central undamaged area (2), at the impact velocity of 555 m/s, the sample shows large area damage, the circular damage area is completely detachment from the matrix, exposing the primer (1) and part of the substrate (2), moreover, part of the substrate is damaged and produced pits (3), the damage area expands to 5.36 mm^2, and when the impact velocity reaches 617 m/s, the coating is completely destroyed, the surface material shows a large area of circular peeling and exposes the primer (1) and most of the substrate (2), and the substrate partially fractures contusion (3), and the damage area increases to 22.22 mm^2. In addition, the repeated test results show that due to the three coatings have no suffer damage at the impact velocity of 360 m/s, it can be judged that at the impact angle of 15°, the velocity threshold of the coating surface is about 360 m/s.

Based on the 3D contour scanning and reconstruction function of the ultra-depth-of-field 3D digital microscope VHX-5000, the local structure of the sample after magnification has been observed, and a high-resolution 3D image capable of analyzing and measuring the sample surface has been created to obtain the damage volume. After obtaining the volume average, the bar chart of the damage volume of the three coatings changes with the impact velocity has been established,

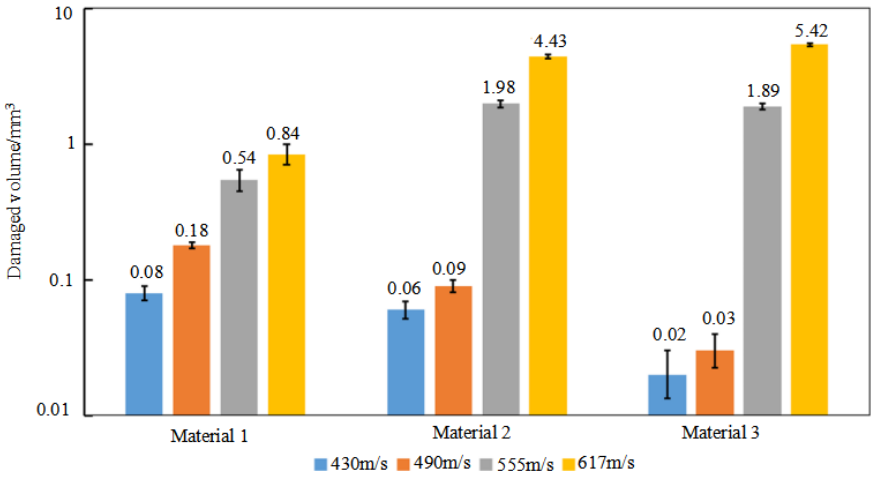

Fig. 9 The relation between the damaged volume and impact velocity

Table 3 The relation between the damaged volume and impact velocity

Coating	Damaged volume/mm^3			
	430 m/s	490 m/s	555 m/s	617 m/s
Material 1	0.08	0.18	0.54	0.84
Material 2	0.06	0.09	1.98	4.43
Material 3	0.02	0.03	1.89	5.42

as shown in the Fig. 9 and in the Table 3. It can be concluded that with the increase of the impact velocity, the damage volume of the coating caused by rain erosion is gradually increasing until the coating sample is completely destroyed. The research results of Gujba (Gujba *et al.* 2016) prove that the higher the impact velocity, the faster the erosion start time and the greater the maximum erosion rate (ERmax), which is related to the impact velocity. SEM microscopic images show that the erosion damage morphology in the early stages is mainly microcracks, bumps and isolated pits with irregular shapes, while in the later stages of droplet erosion, the peeling of coating materials is mainly caused by hydraulic penetration.

In previous studies, Imeson *et al.* (Imeson *et al.* 1981, Nearing *et al.* 1986) obtain the linear relation between the output signal voltage and the instantaneous value of the impact force by drawing the function image of the output signal voltage and the instantaneous value of the impact force, obtaining the linear relation between the two under different droplet diameters, and propose the instantaneous approximate formula of the impact force generated by droplet impact

$$F = \frac{mv^2}{d}. \tag{5}$$

With F being the impact force, v is the impact velocity of the droplet, m and d are the mass and diameter of the droplet. It can be known from the above formula that under the same droplet diameter and mass, the impact velocity determines the impact force, that is, the greater the impact velocity, the greater the instantaneous impact force generated when the droplet contacts the sample, ultimately leading to a gradual deepening of the damage degree.

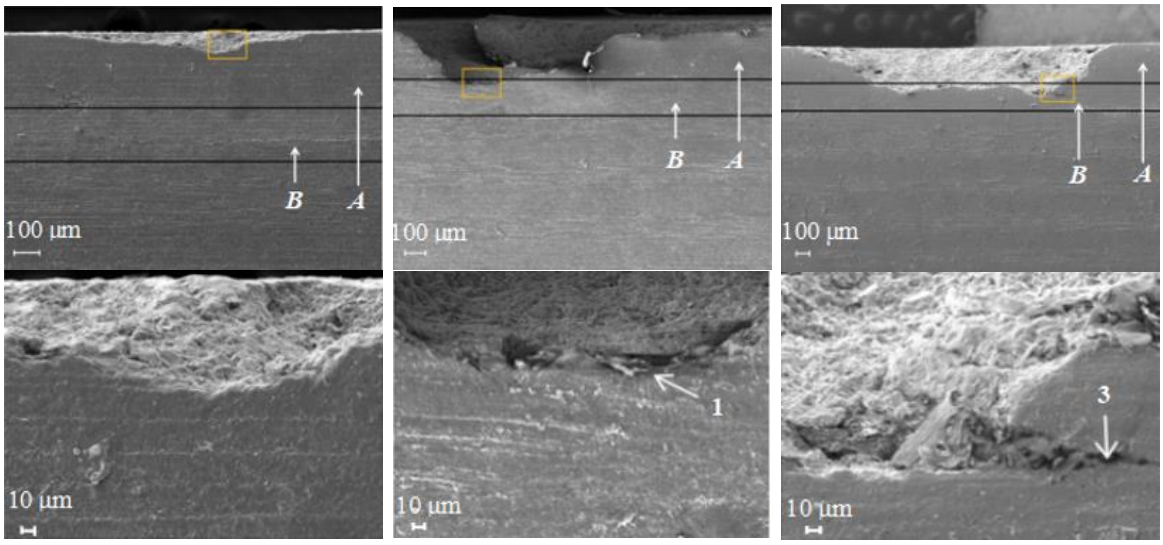

490 m/s 555 m/s 617 m/s

(a) Material 1

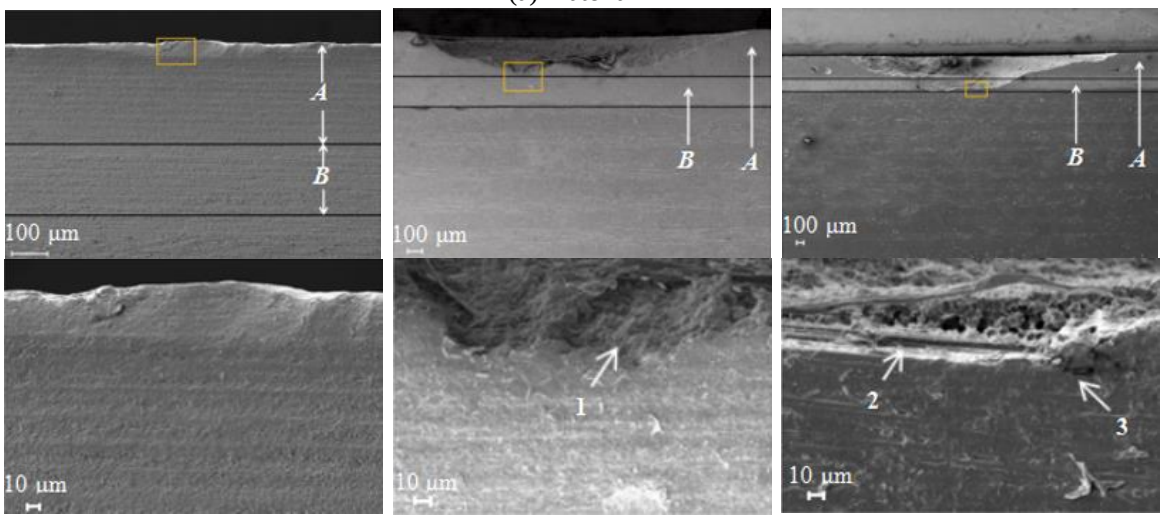

490 m/s 555 m/s 617 m/s

(b) Material 2

Fig. 10 SEM micrographs of the three kinds of coatings damaged with various impact velocities at an impact angle of 15°

In addition, among the three samples, the damage volume growth of the material 1 coating is more stable than that of the other two coatings, while the damage of the material 2 and material 3 coatings accelerates sharply after the speed of 490 m/s. According to the relation between surface roughness and erosion initiation, at the same impact velocity, even though the coating material 1 has the largest modulus and hardness and the best mechanical properties, the uneven protrusions on its surface will cause an increase in stress, making the material more prone to initial erosion damage, although the coating material 3 has the worst mechanical properties, its surface is

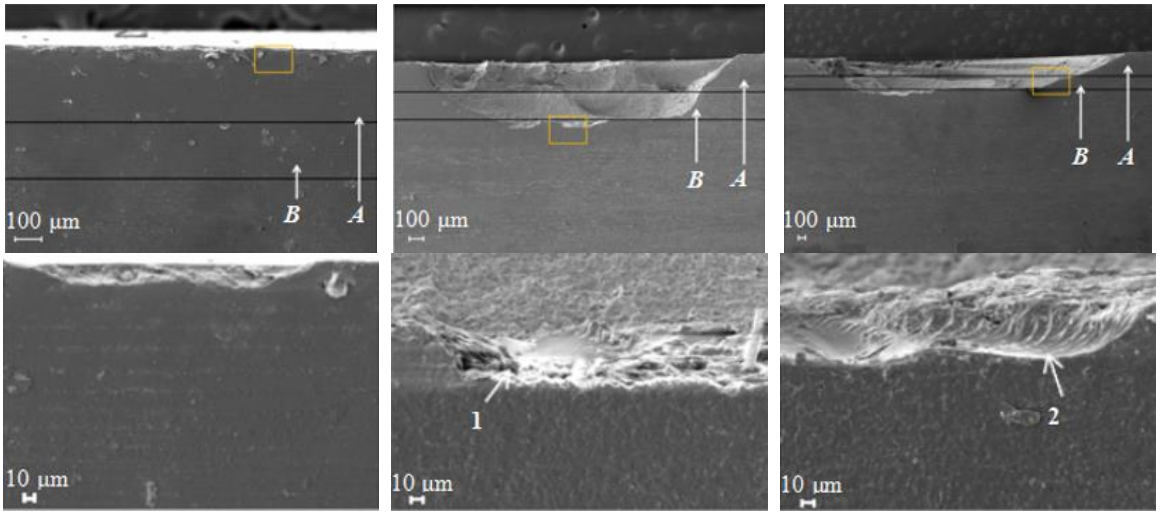

490 m/s 555 m/s 617 m/s

(c) Material 3

Fig. 10 Continued

relatively smooth, so it is not easy to form initial erosion damage. The greater damageability of a rougher surface compared to a smooth surface is explained by the fact that greater roughness causes the formation of large surface and internal stresses. When these stresses reach the tensile strength of the material, there is a destruction. The results prove that the surface roughness is the main reason for the initial erosion damage of the coating material.

Comparing the Fig. 10, it can be found that the area of delamination damage can be several times the size of the surface damage, so for the high-speed rain erosion damage of coating materials, it is not accurate enough to directly quantify the degree of rain erosion damage on the surface annular damage. In order to more intuitively characterize the effect of raindrop impact velocity on the rain erosion damage of the coating, the sample was cut along the axis of the annular damage on the surface with a diamond wire saw, and then the cross-sectional morphology of the damaged area of the sample has been observed by the SEM scanning electron microscope. The Fig. 10 shows the SEM cross-sectional microscopic images of the three coatings at velocities of 490 m/s, 555 m/s and 617 m/s, the first row is the observation image of the overall damage morphology, The second row is the locally enlarged damage morphology observation image of the yellow frame marked area. In the figure, A is the topcoat area, B is the primer area, the rest is the substrate area. It can be seen that as the speed increases, the damage depth also gradually increases, at a speed of 490 m/s, the damage mainly exists in the topcoat area (*A*), showing irregular and slight scratches, at a speed of 555 m/s, the damage reaches the primer area (*B*), and at this time, pits (1) are formed due to the peeling of the coating, when the speed reaches 617 m/s, the damage extends to the substrate area, and the surface has obvious micro-ploughing damage (2). In coating material 1, significant cracks can be observed (3). From the formulas (1), (2) and (3), it can be seen that with the increase of the impact velocity, the stress wave intensity gradually increases, the water hammer pressure becomes larger, and the amplitude generated by normal incident, reflected, and transmitted stress waves at the liquid-coating interface and coating-substrate interface leads to damage and failure of the coating.

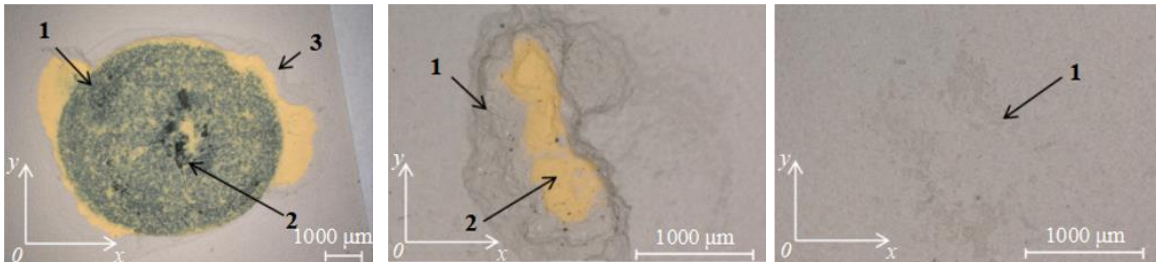

(a) 0° (b) 15° (c) 30°

Fig. 11 Damage morphology of coating material 1 with various impact angles

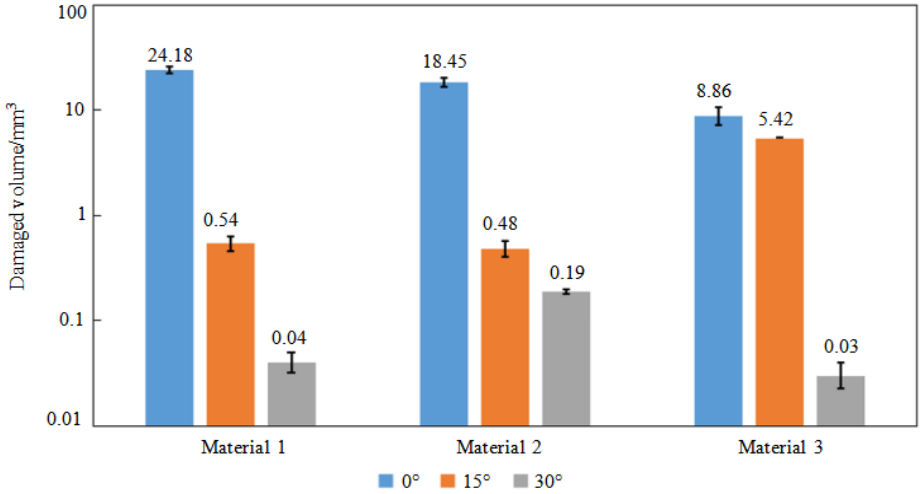

Fig. 12 The relation between the damaged volume and impact angle

Table 4 The relation between the damaged volume and impact angle

Coating	Damaged, volume/mm^3		
	0°	15°	30°
Material 1	24.18	0.54	0.04
Material 2	18.45	0.48	0.19
Material 3	8.86	5.42	0.03

3.2.3 Impact test results at different jet angles

The Fig. 11 is the electron microscopic typical damage microscopic images of coating material 1 at the impact velocity of 617 m/s and the impact angles of 0°, 15°, and 30°. It can be seen that at the impact angle of 0°, the sample shows a large area of peeling damage, the matrix is completely exposed (1), and the matrix is partially broken with slight contusion (2), and the periphery shows ring-shaped wave damage (3), the coating is completely destroyed, with a damage area of 42.18 mm^2, however, at the impact angle of 15°, the sample shows a band-like wave damage (1), with pits in the central area and exposed topcoat (2), and the damage area decreases to 2.57 mm^2 compared to 0° impact angle, when the impact angle is 30°, the damage of the sample shows slight abrasion on the surface (1), and the damage area is only 1.56 mm^2.

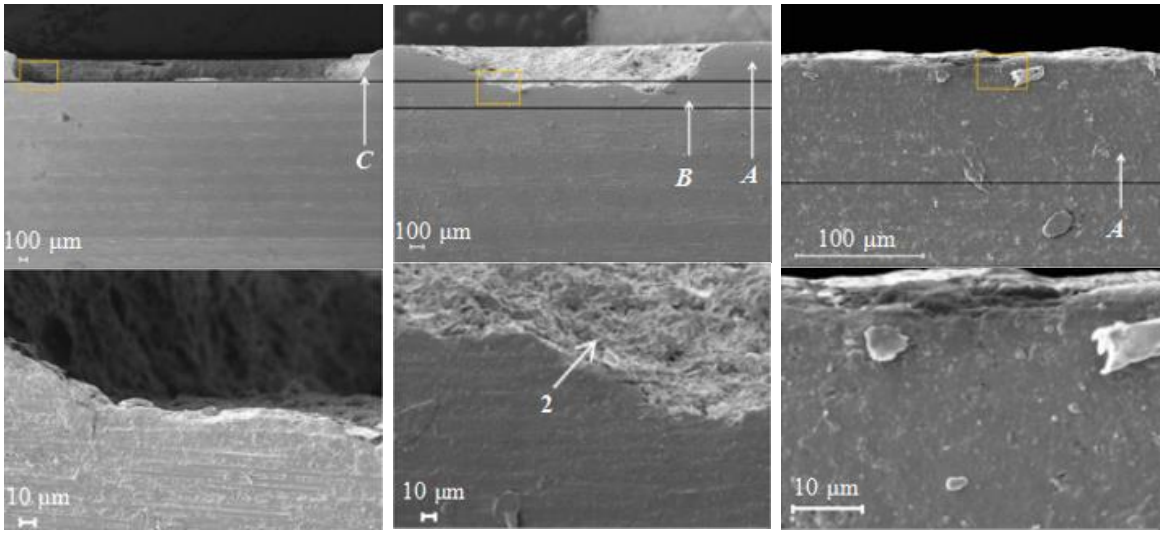

0° 15° 30°

(a) Material 1

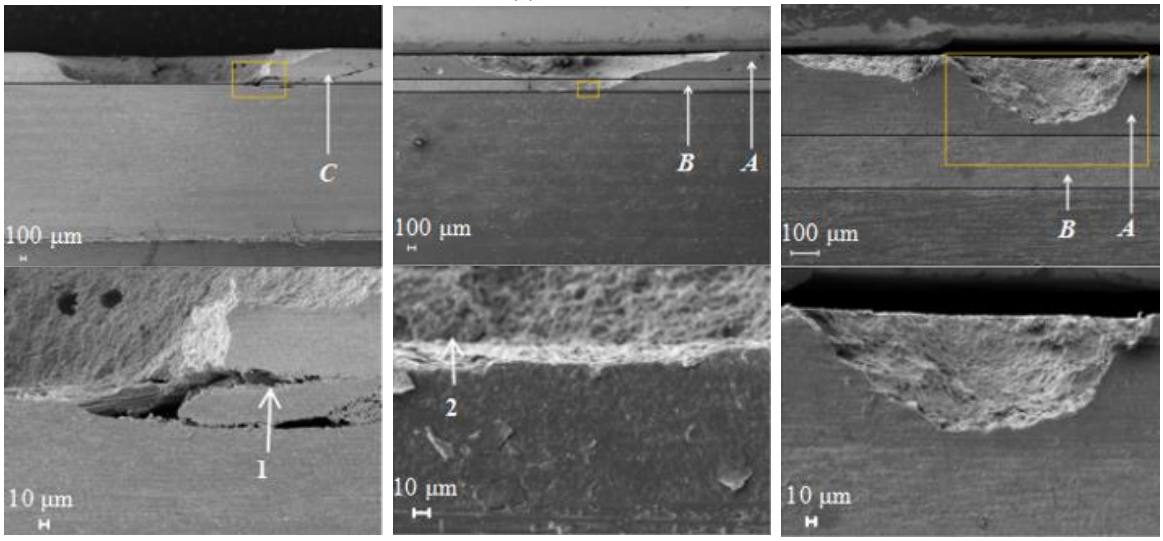

0° 15° 30°

(b) Material 2

Fig. 13 SEM micrographs of the three kinds of coatings damaged with various impact angle at an impact velocity of 617 m/s

Based on the 3D contour scanning and reconstruction function of the ultra-depth-of-field 3D digital microscope VHX-5000, the average value is obtained after measuring the damage volume, and the bar chart of three kinds of coating damage volume changes with impact angle is established. The Fig. 12 and the Table 4 shows the observed variation of damage volume of three coating samples with jet impact angle. It can be concluded that as the increase of the impact angle, the damage of the coating caused by rain erosion is gradually weakened until almost no damage

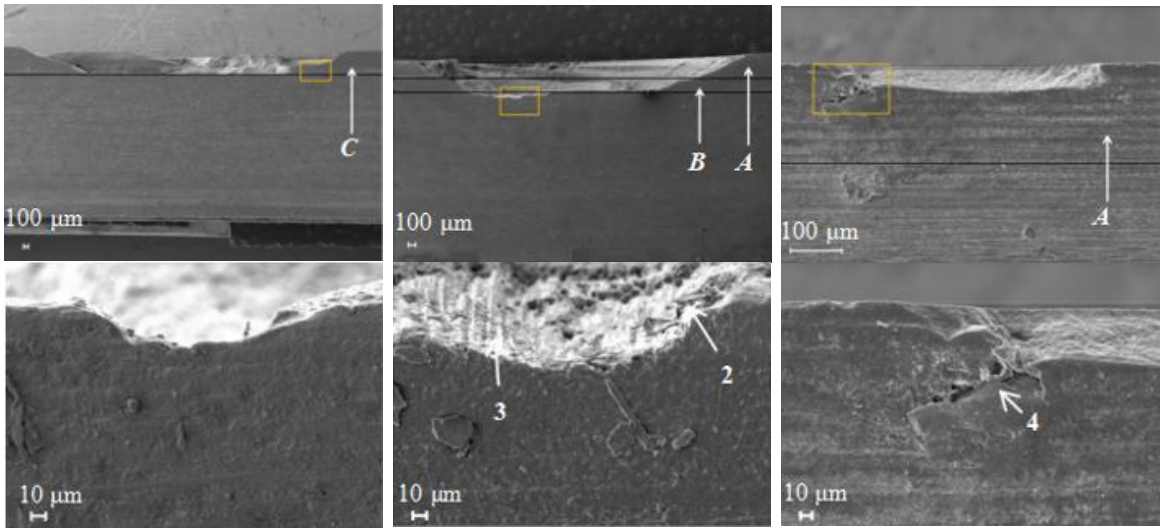

0° 15° 30°

(**c**) Material 3

Fig. 13 Continued

occurs on the coating sample. The reason is that the degree of damage is mainly related to the velocity component perpendicular to the specimen. As the impact angle increases, the component of the impact velocity in the vertical direction gradually decreases, resulting in a gradual decrease in the degree of damage, in addition, as the included angle increases, the liquid-solid contact continues on the surface before the droplet is compressed and released. The time also increases, resulting in a decrease in the impact pressure (Shi and Dear 1992), which is also the main reason for this damage trend.

The Fig. 13 shows the SEM cross-sectional morphology observation images of the damage of three samples at the impact angles of 0°, 15° and 30° at the speed of 617 m/s. It can be seen that as the impact angle increases, the depth of damage decreases continuously. At the impact angle of 0°, the coating damage area (*C*) is completely peeled off and destroyed, the substrate is exposed in a large area, and the damage profile presents a platform shape. In the SEM scanning electron micrograph of the coating material 2, the delamination cracks (1) due to the action of shear waves can be clearly observed, at the impact angle of 15°, the damage of the three coatings exhibits conical cross-sections, irregular pits (2) and plowing marks (3) due to coating peeling can be observed under high-magnification observation, and the damage extends to the primer area (*B*), and the substrate is exposed in some areas, At the impact angle of 30°, the coating damage occurs only in the topcoat area (*A*). In the high-magnification observation image of coating material 3, the initial cracks on the coating topcoat caused by the water hammer pressure can be observed (4). The different damage situations mentioned above are due to the greater impact of stress wave reflection and transmission at smaller impact angles, resulting in delamination and then peeling of the interface, but as the impact angle increases, the intensity of the stress wave weakens, and the damage gradually decrease.

It is obvious that in the design of the aircraft skin it is advisable to use more durable, hard and wear-resistant coatings that prevent destruction from external influences.

4. Conclusions

In this investigation, a single-jet rain erosion test platform is built based on a first-stage light gas cannon, which can produce a stable water jet in the shape of a mushroom head with a diameter of 200-700 m/s and a diameter of 4-7 mm. Under the condition of different jet velocity and angle, single jet impact test is carried out for three kinds of aircraft skin coatings with the same thickness. The test results show that the typical damage of a single water jet impact on the skin coating has the following rules:

(1) The three skin coatings exhibit almost the same damage mode when subjected to jet impact. Mainly manifested as surface abrasion at low speed and interface delamination damage at high speed,

(2) At the same impact angle, as the impact velocity increases, the damage area of the three coating samples gradually increases, and gradually transitions from slight abrasion to peeling damage. The coating is more prone to large-area delamination damage at the high velocity,

(3) At the same impact velocity, as the impact angle increases, the normal velocity component gradually decreases, and the instantaneous impact force of the droplet contacting the material surface also decreases with the generation of the velocity component, resulting in initial damage Finally, the damage area of the three coating samples is gradually reduced, from the obvious damage at 0° to the slight scratch at 30°, or even no damage,

(4) The threshold velocity for erosion damage to the single-jet impingement coating is about 360 m/s. The early stages of erosion damage morphology are mainly microcracks, bumps, and isolated pits of irregular shape, while in the late stage of droplet erosion, the peeling mode of the material is caused by hydraulic permeation.

(5) At the same impact velocity and angle of the three coating samples, although coating material 1 has the best mechanical properties, its surface is the roughest, so the initial erosion damage is the most obvious, although the mechanical properties of coating material 3 is the worst, but its surface is the smoothest, so it is the least prone to initial erosion damage. It can be seen that surface roughness is the main factor affecting the degree of rain erosion damage of materials in their own characteristic parameters.

The obtained results help to better study the physics of the aircraft skin damage process, design the most resistant coating to external influences and select the most effective non-destructive testing method during operation and repair, for example, the acoustic or X-ray methods.

Acknowledgement

This work was supported by the National Natural Science Foundation of China (Nos. 12261131505, 11832015), Basic Research Programs of Taicang (Nos. TC2020JC30).

References

Adler, W.F. (1999), “Rain impact retrospective and vision for the future”, *Wear*, **233**, 25-38. https://doi.org/10.1016/S0043-1648(99)00191-X.

Bech, J.I., Johansen, N.F.J., Madsen, M.B., Hannesdóttir, Á. and Hasager, C.B. (2022), “Experimental study on the effect of drop size in rain erosion test and on lifetime prediction of wind turbine blades”, *Renew.*

Energy, **197**, 776-789. https://doi.org/10.1016/j.renene.2022.06.127.
Cook, S.S. (1928), "Erosion by Water-Hammer", *Proc. Roy. Soc. London*, **119**(783), 481-488. https://doi.org/10.1016/S0016-0032(29)91613-6.
Coto, B., Hallander, P., Mendizabal, L., Pagano, F., Kling, H., Ortiz, R., Barriga, J. and Selegård, L. (2021), "Particle and rain erosion mechanisms on Ti/TiN multilayer PVD coatings for carbon fibre reinforced polymer substrates protection", *Wear*, **466**, 203575. https://doi.org/10.1016/j.wear.2020.203575.
Dear, J.P. and Field, J.E. (1988), "High-speed photography of surface geometry effects in liquid/solid impact", *J. Appl. Phys.*, **63**(4), 1015-1021. https://doi.org/10.1063/1.340000.
Field, J.E. (1986), "Liquid impact erosion", *Phys. Bull.*, **37**(2), 70-72. https://doi.org/10.1088/0031-9112/37/2/027.
Field, J.E., Dear, J.P. and Ogren, J.E. (1989), "The effects of target compliance on liquid drop impact", *J. Appl. Phys.*, **65**(2), 533-540. https://doi.org/10.1063/1.343136.
Gohardani, O. (2011), "Impact of erosion testing aspects on current and future flight conditions", *Progr. Aerosp. Sci.,* **47**(4), 280-303. https://doi.org/10.1016/j.paerosci.2011.04.001.
Gujba, A.K., Hackel, L., Kevorkov, D. and Medraj, M. (2016), "Water droplet erosion behaviour of Ti-6Al-4V and mechanisms of material damage at the early and advanced stages", *Wear*, **358**, 109-122. https://doi.org/10.1016/j.wear.2016.04.008.
Heymann, F.J. (1968), "On the shock wave velocity and impact pressure in high-speed liquid-solid impact", *J. Bas. Eng.*, **90**(3), 400-402. https://doi.org/10.1115/1.3605114.
Imeson, A.C., Vis, R. and Water, D.E. (1981), "The measurement of water-drop impact forces with a piezo-electric transducer", *Catena*, **8**, 83-96. https://doi.org/10.1016/S0341-8162(81)80006-9.
Itoh, H. and Okabe, N. (1993), "Evaluation of erosion by liquid droplet impingement for metallic materials", *Trans. JPN Soc. Mech. Eng. Part A*, **59**(567), 2736-2741. https://doi.org/10.1299/kikaia.59.2736.
Jenkins, D.C. (1955), "Erosion of surfaces by liquid drops", *Nature*, **176**(4476), 303-304. https://doi.org/10.1038/176303a0.
Keegan, M.K., Nash, D.H. and Stack, M.M. (2013), "On erosion issues associated with the leading edge of wind turbine blades", *J. Phys. D: Appl. Phys.*, **46**(38), 383001. https://doi.org/10.1088/0022-3727/46/38/383001.
Kennedy, C.F. and Field, J.E. (2000), "Damage threshold velocities for liquid impact", *J. Mater. Sci.*, **35**(21), 5331-5339. https://doi.org/10.1023/A:1004842828161.
King, R.B. (1976), "Erosion by liquid impact", *Aeronaut. J.*, **80**(791), 492-493. https://doi.org/10.1017/S0001924000034552.
Lan, L.F., Xian, Y. and Fu, M.Y. (2014), *Oil and Coating Testing Technology*, Chemical Industry Press, Beijing, China.
Li, Y. (2008), "Failure analysis of corrosion protection coating", *Shanghai Coat.*, **46**(9), 36-39. https://doi.org/10.3969/j.issn.1009-1696.2008.09.012.
Mednikov, A.F., Tkhabisimov, A.B., Filatov, A.A. and Lukyanychev, D.A. (2021), "Forecasting the service life of paint coatings under conditions simulating aircraft flight modes in a dusty atmosphere and under the influence of rain load", *Materials of the VI All-Russian Scientific and Technical Conference*, Moscow, Russia, May.
Mishnaevsky Jr, L. (2019), "Toolbox for optimizing anti-erosion protective coatings of wind turbine blades: overview of mechanisms and technical solutions", *Wind Energy*, **22**(11), 1636-1653. https://doi.org/10.1002/we.2378.
Nearing, M.A., Bradford, J.M. and Holtz, R.D. (1986), "Measurement of force vs. time relations for waterdrop impact", *Soil Sci. Soc. Am. J.*, **50**(6), 1532-1536. https://doi.org/10.2136/sssaj1986.03615995005000060030x.
Obara, T.B.N.K.F., Bourne, N.K. and Field, J.E. (1995), "Liquid-jet impact on liquid and solid surfaces", *Wear*, **186**, 388-394. https://doi.org/10.1016/0043-1648(95)07187-3.
Richman, R.H. (2002), *Liquid-Impact Erosion*, ASM Handbook, Vol. 11, 1013-1018.
Schmitt, G.F. (1974), "Materials parameters that govern the erosion behavior of polymeric composites in subsonic rain environments", ASTM International, Montgomery County, USA.

Schramm, M., Rahimi, H., Stoevesandt, B. and Tangager, K. (2017), "The influence of eroded blades on wind turbine performance using numerical simulations", *Energi.*, **10**(9), 1420. https://doi.org/10.3390/en10091420.

Shi, H.H. and Dear, J.P. (1992), "Oblique high-speed liquid-solid impact", *JSME Int. J.*, **35**(3), 285-295. https://doi.org/10.1299/jsmea1988.35.3_285.

Slot, H.M., Gelinck, E.R.M., Rentrop, C. and Van Der Heide, E. (2015), "Leading edge erosion of coated wind turbine blades: Review of coating life models", *Renew. Energy*, **80**, 837-848. https://doi.org/10.1016/j.renene.2015.02.036.

Springer, G.S. (1974), "Analysis of rain erosion of coated materials", *J. Compos. Mater.*, **8**(3), 229-252. https://doi.org/10.1177/002199837400800302.

Tobin, E.F., Young, T.M., Raps, D. and Rohr, O. (2011), "Comparison of liquid impingement results from whirling arm and water-jet rain erosion test facilities", *Wear*, **271**(9-10), 2625-2631. https://doi.org/10.1016/j.wear.2011.02.023.

Valaker, E.A., Armada, S. and Wilson, S. (2015), "Droplet erosion protection coatings for offshore wind turbine blades", *Energy Procedia*, **80**, 263-275. https://doi.org/10.1016/j.egypro.2015.11.430.

Ying, Y. and Xu, G.D. (2011), "Development of pitch control for load reduction on wind turbines", *J. Mech. Eng.*, **47**(16), 106-111. https://doi.org/10.3901/JME.2011.16.106.

Young, T.M. and Humphreys, B. (2001), "Fielding investigation of Hybrid Laminar Flow Control (HLFC) surfaces", *Aircraft Des.*, **4**(2/3), 127-146. https://doi.org/10.1016/S1369-8869(01)00010-6.

Zahavi, J. and Nadiv, S. (1981), "Indirect damage in composite materials due to raindrop impact", *Wear*, **72**, 305-313. https://doi.org/10.1016/0043-1648(81)90257-X.

Zhang, S., Dam-Johansen, K., Nørkjær, S., Bernad Jr, P.L. and Kiil, S. (2015), "Erosion of wind turbine blade coatings-Design and analysis of jet-based laboratory equipment for performance evaluation", *Progr. Organ. Coat.*, **78**, 103-115. https://doi.org/10.1016/j.porgcoat.2014.09.016.